3D edge impurity transport analysis using the EMC3-EIRENE code by taking into account multiple edge plasma measurements on W7-X

Y. Luo[1], Y. Liang[1], S. Xu[1], E. Wang[1], M. Krychowiak[2], D. Gradic[2], E. Flom[2], F. Henke[2], O. Neubauer[1], P. Drews[1], A. Knieps[1], J. Liu[1], D. Reiter[3], D. Harting[1], Y. Feng[2], F. Reimold[2], G. Fuchert[2], and the W7-X Team

[1] *Forschungszentrum Jülich GmbH, Institut für Energie- und Klimaforschung - Plasmaphysik, 52425 Jülich, Germany*

[2] *Max Planck Institute for Plasma Physics, 17491 Greifswald, Germany*

[3] *Institute for Laser and Plasma Physics, Heinrich-Heine-University, D-40225 Düsseldorf, Germany*

Introduction

As more edge diagnostics of FZJ are employed on W7-X (such as divertor spectroscopy endoscopes, reflectometry, multi-purpose manipulator), comparison of their measurements to simulations with the code EMC3-EIRENE becomes more important and useful. The comparison of EMC3-Eirene simulation results and some local diagnostics has been already quantitatively analysed on W7-X [1-3]. For example, M. Krychowiak compared 2D emissions CII (712 nm) and CIII (674 nm) at the divertor with EMC3-EIRENE [2]. This work focuses on the comparison of divertor spectrometer measurements with EMC3-EIRENE simulations. The purpose is mutual validation of diagnostics and simulations. Impurity line emissions can be used to analyse impurity transport, as they contain the information of electron temperature, electron density and impurity concentration. To better match the experimental data, radially dependent cross-field transport coefficients are used in EMC3-EIRENE simulations. In addition, previous studies show that finite plasma beta can affect edge stochastization [3,4], and toroidal currents can shift the magnetic islands in the W7-X SOL [5]. In order to obtain more reliable output parameters or prediction results, the equilibrium effects (including plasma beta and current effects) on edge magnetic topologies have been considered in EMC3-EIRENE by integrating with HINT code [6].

Tools and methods

Divertor spectroscopy observation at W7-X utilizes several spectrometers viewing one upper and one lower divertor with horizontal and vertical lines of sight (LOS) [2]. Measurements used in this work were taken along the horizontal LOS at the upper divertor in standard configuration. Two

spectrometers are used to measure CII (426.83 nm), CIII (465.01 nm), hydrogen Balmer series and molecular line emissions during W7-X OP 1.2b. As shown in Figure 1 (a), the view consists of 27 LOS channels ranging from 0.5 to 14.5 cm above the horizontal target plates at the toroidal angle of $\phi = -59.69°$. Figure 1 (b) shows the spectrum observed by SP2750 spectrometer for discharge #20180919.025. CII and H_γ are used to compare with simulations, because both CII and H_γ can reflect electron density and temperature information, and CII also provides C^+ information. Thomson Scattering (TS) can provide radial profiles of n_e and T_e at the toroidal angle of $\phi = 170.5°$.

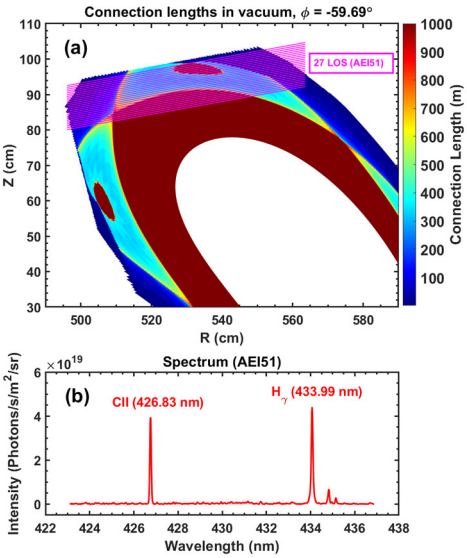

Figure 1. (a) Horizontal LOS of Divertor spectroscopy at the AEI51 Port, (b) spectrum of one observation channel for discharge #20180919.025.

In general, line emission is composed of three parts: excitation, recombination, and charge exchange.

$$\epsilon_{i\to j} = \sum_{\sigma} PEC^{(exc)}_{\sigma,i\to j} n_e n_\sigma^{z+} + \sum_{\rho} PEC^{(rec)}_{\rho,i\to j} n_e n_\sigma^{(z+1)+} + \sum_{\rho} PEC^{(CX)}_{\rho,i\to j} n_H n_\sigma^{(z+1)+} \quad (\text{photons cm}^{-3}\text{s}^{-1})$$

Where PEC represents photon emissivity coefficient, σ metastable, n_e electron density, n_σ^{z+} density of the z-times ionized ion. Three types of PEC coefficients used in this work are from the generalized collisional–radiative model [7].

Comparison of edge measurements with simulations

In this work, a standard configuration program (#20180919.025) with ECRH heating is chosen for analysis. The main plasma parameters of selected shot are ECRH heating power P_{ECRH} = 4.0 MW, radiation power P_{rad} = 0.75 MW, toroidal plasma current I_p = 3 kA. In simulation, heating power is set to 3.6 MW. For this discharge, H_γ (433.99 nm) and CII were measured by divertor spectroscopy. As shown in Table 1, for cases 1-3, the separatrix density is scanned at fixed constant cross-field transport coefficients. For case 4-6, transport coefficients are varied at a fixed separatrix density. Figure 2 shows experimental data (Thomson

Table 1. The input separatrix density and cross-field transport coefficients in different cases

Case	n_{es} (10^{19} m^{-3})	D (m^2/s)	χ (m^2/s)
Case 1	2.0	0.5	3*D
Case 2	2.2	0.5	3*D
Case 3	2.5	0.5	3*D
Case 4	2.2	0.3 (r_{eff}<1), 0.4 (r_{eff} ≥1)	3*D
Case 5	2.2	0.8 (r_{eff}<1), 0.3 (r_{eff} ≥1)	3*D
Case 6	2.2	0.3 (r_{eff}<1), 1.0 (r_{eff} ≥1)	3*D

scattering data in figure 2(a, b), spectrometer data in figure 2(c, d)) and simulation results in cases 1-3. It indicates that the results of case 3 are consistent with the spectrometer measurements, but deviate from the CII and TS data. Therefore, the next step is to try to reduce separatrix density and adjust cross-field transport coefficients. As shown in figure 3, when we reduce separatrix density and cross-field transport coefficients inside LCFS in case 3, Thomson scattering data matches better with simulations, but H_γ is larger than simulation. This could be due to the simulation electron density in the volume of LOS being lower than the experimental electron density. To approach the experiment, the equilibrium magnetic field considering toroidal plasma current and finite beta are given respectively by Hint code. Figure 4 shows experimental data and simulation results at three different magnetic fields (Vacuum, I_p = 3 kA, axis beta = 2%) using the same input parameters as in case 4. For Case axis beta =2%, the edge density increases and H_γ matches better with experimental data, whereas for case I_p = 3 kA, n_e, T_e and H_γ change less. It indicates that the toroidal plasma current has a weak effect on the edge electron temperature and density distribution, while finite beta significantly changes T_e and n_e. Figure 5 shows that finite beta changes the magnetic island size and redistributes the C^{3+} concentration. Although plasma toroidal current also shifts the magnetic island away from the target plates, C^{3+} distribution nearly keeps unchanged compared to the vacuum field case.

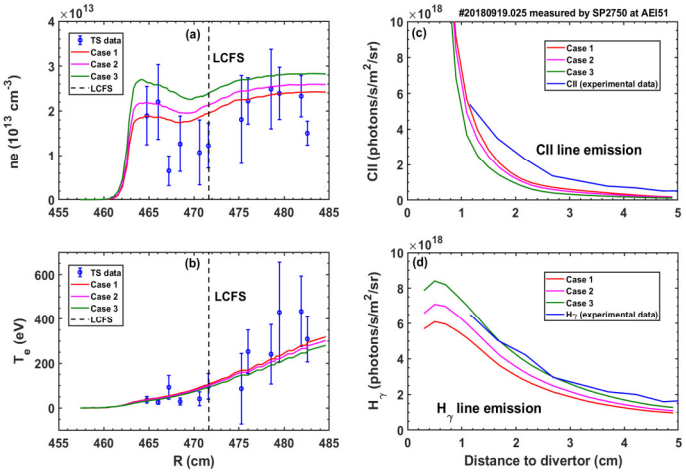

Figure 2. Experimental data and simulation results in case 1-3: (a) electron density, (b) electron temperature, (c) CII line emission, (d) H_γ line emission

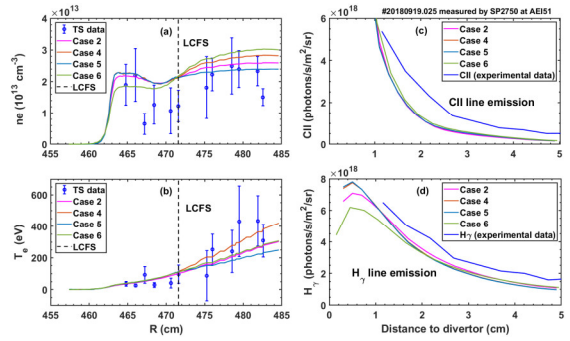

Figure 3. Experimental data and simulation results in case 2, 4-6.

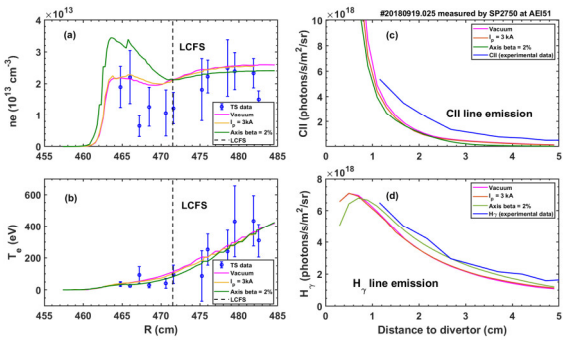

Figure 4. Experimental data and simulation results at three different magnetic configurations (Vacuum, I_p=3 kA, axis beta=2%).

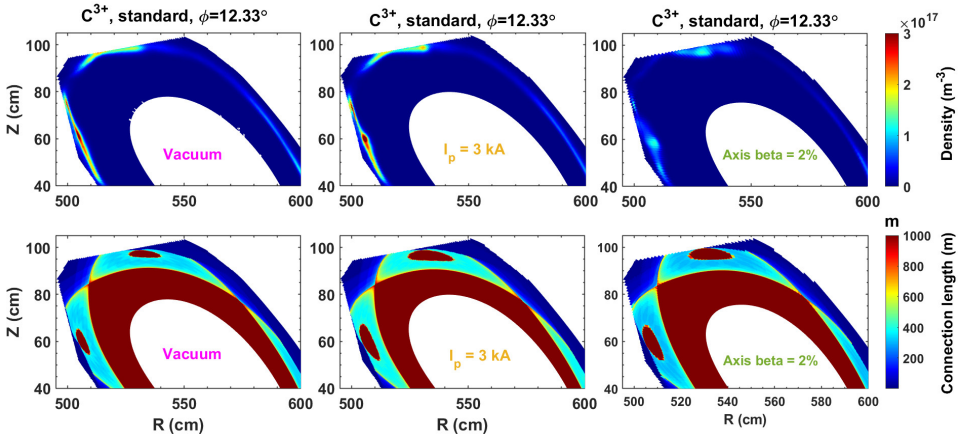

Figure 5. C^{3+} distributions and connection lengths in different magnetic configurations

Summary

The intensity distributions of CII (426.83 nm) and hydrogen Balmer series measured by divertor spectrometers are used to validate the EMC3-EIRENE simulations. By adjusting the transport coefficients and considering the equilibrium effects on the simulations, it shows that measured H_γ is in good agreement with the simulation results, but CII is not. Perhaps the carbon sources and carbon transport coefficients are not set correctly, more works are needed to match measured CII line emission and simulation results. Obviously, equilibrium effects change magnetic topologies and have effects on edge density, temperature and carbon concentration distribution. Especially, finite beta increases SOL electron density.

Acknowledgements

This work has been carried out within the framework of the EUROfusion Consortium, funded by the European Union via the Euratom Research and Training Programme (Grant Agreement No 101052200 — EUROfusion). Views and opinions expressed are however those of the author(s) only and do not necessarily reflect those of the European Union or the European Commission. Neither the European Union nor the European Commission can be held responsible for them.

Yu Luo gratefully acknowledges funding from China Scholarship Council.

Reference

[1] Y. Feng *et al.*, Nucl Fusion **61**, 106018 (2021).
[2] M. Krychowiak *et al.*, *European Conference on Plasma Physics* (2021).
[3] S. Xu *et al.*, Nucl Fusion **63** (2023).
[4] S. Zhou *et al.*, Nucl Fusion **62**, 106002 (2022).
[5] Y. Gao *et al.*, Nucl Fusion **59** (2019).
[6] F. Effenberg *et al.*, Nucl Mater Energy **18**, 262 (2019).
[7] H. P. Summers *et al.*, Plasma Phys Contr F **48**, 263 (2006).